Title
The structure of tomato aspermy virus by X-ray crystallography

Journal
Journal of Structural Biology, 139(2)

ISSN
1047-8477

Authors
Lucas, Robert W
Larson, Steven B
Canady, Mary A
et al.

Publication Date
2002-10-01

DOI
10.1016/s1047-8477(02)00561-0

ACADEMIC PRESS

Available online at www.sciencedirect.com

SCIENCE DIRECT®

Journal of Structural Biology 139 (2002) 90–102

Journal of Structural Biology

www.academicpress.com

The structure of tomato aspermy virus by X-ray crystallography

Robert W. Lucas, Steven B. Larson, Mary A. Canady,[1] and Alexander McPherson*

Department of Molecular Biology and Biochemistry, University of California, Irvine, Irvine, CA 92697-3900, USA

Received 12 March 2002, and in revised form 17 June 2002

Abstract

The three-dimensional structure of tomato aspermy virus (TAV) has been solved by X-ray crystallography and refined to an *R* factor of 0.218 for 3.4–40 Å data (effective resolution of 4 Å). Molecular replacement, using cucumber mosaic virus (Smith et al., 2000), provided phases for the initial maps used for model building. The coat protein of the 280 Å diameter virion has the canonical "Swiss roll" β-barrel topology with a distinctive amino-terminal α-helix directed into the interior of the virus where it interacts with encapsidated RNA. The N-terminal helices are joined to the β-barrels of protein subunits by extended polypeptides of six amino acids, which serve as flexible hinges allowing movement of the helices in response to local RNA distribution. Segments of three nucleotides of partially disordered RNA interact with the capsid, primarily through arginine residues, at interfaces between A and B subunits. Side chains of cys64 and cys106 form the first disulfide observed in a cucumovirus, including a unique cysteine, 106, in a region otherwise conserved. A positive ion, putatively modeled as a Mg^{+} ion, lies on the quasi-threefold axis surrounded by three quasi-symmetric glutamate 175 side chains.

Keywords: Cucumovirus; Diffraction; Disulfide bridge; Metal ions; Nucleoprotein

1. Introduction

Tomato aspermy virus (TAV), a member of the cucumovirus genus, is a $T = 3$ spherical plant virus of $M_r = 4.6 \times 10^6$ that infects a broad range of plants in the wild including dicotyledonous and monocotyledonous families (Hollings and Stone, 1971). Its capsid is composed of 180 polypeptides of identical sequence and organized as a 280 Å diameter icosahedron with 60 copies each of three conformationally distinct subunits designated A, B, and C. Twelve pentameric capsomeres are composed of A subunits, and 20 hexameric capsomeres of B and C subunits. The coat protein has a molecular weight of 24 096 Da and a length of 217 amino acids (O'Reilly et al., 1994). Structurally, the virus is very closely related to cucumber mosaic virus (CMV), the type member of the *Cucumovirus* genus, whose three-dimensional structure has been determined (Smith et al., 2000).

TAV has a tripartite, positive sense, single-stranded RNA genome with molecular weight components of $M_r = 1.26 \times 10^6$ for RNA1, 1.10×10^6 for RNA2, and 0.90×10^6 for RNA3, as well as a subgenomic fragment of RNA3, designated RNA4, of $M_r = 0.43 \times 10^6$ Da. RNA4, packaged in virions along with RNA3, contains only an open-reading frame for the coat protein. The complete nucleotide sequence of the genome is known, and from that, the amino-acid sequence of the coat protein (O'Reilly et al., 1994). As in all members of the *Cucumovirus* genus, the RNAs of TAV have 5′ caps and conserved 3′ termini of about 200 nucleotides, but lack poly(A) tails. Instead, the 3′ termini assume tRNA-like structures that can be aminoacylated with tyrosine (Van Regenmortel et al., 2000). The amino-acid sequences of TAV and CMV are 42% identical, resulting in structural similarity, cross-protection in plants for certain isolates, and cross-reactivity to antibodies (Savithri et al., 1984).

* Corresponding author. Fax: +949-824-1954.
E-mail address: AMCPHERS@uci.edu (A. McPherson).
[1] Current address: Invitrogen Corp., 1600 Faraday Avenue, Carlsbad, CA 92008.

1047-8477/02/$ - see front matter © 2002 Elsevier Science (USA). All rights reserved.
PII: S1047-8477(02)00561-0

2. Materials and methods

2.1. Preparation of virus

Tomato aspermy virus (TAV), Blencowe strain, was obtained from the American Type Culture Collection (Rockville, MD). Virus was propagated in *Nicotiana clevelandii* in a greenhouse maintained at a temperature of 20–30 °C. Infectious material was ground with a mortar and pestle at 4 °C and suspended in 20 mM Tris at pH 7.0 and about 0.2%(w/v) thioglycollic acid. Plants having leaves about 5 cm long were infected by gently abrading leaves with cellite and rubbing virus suspension into the wound using a cotton swab. Infected leaves were harvested 2 weeks after inoculation and stored at −20 °C before purification.

Purification of TAV was based on the method of Lot et al. (1972) and was carried out in a 4 °C cold room using prechilled equipment and solutions. About 50 g of frozen, infected *N. clevelandii* leaves were mixed with 100 ml of 0.5 M sodium citrate buffer at pH 6.5 and 0.5% sodium thioglycolate in a Waring blender. After the plant material had been homogenized, 100 ml of cold chloroform was added and the mixture was blended for an additional 2 min before being sieved through two layers of cheesecloth. The solution was then clarified by centrifuging at 5200*g* in a GSA rotor for 10 min at 4 °C. The upper, aqueous layer was carefully removed with a pipette (the bottom, organic layer, was discarded) and 8% polyethylene glycol 8000 was added. The solution was mixed overnight. The virus was then pelleted by centrifuging at 5700*g* in an SS34 rotor at 4 °C for 20 min. The virus pellet was dissolved overnight in 10 ml of 20 mM Tris buffer at pH 7.0. The solution was again clarified by centrifuging at 9400*g* in an SS34 rotor for 20 min and the pellet was discarded. Virus was then pelleted at 61 000*g* in a Beckman NVT90 rotor for 2.5 h at 4 °C. The pellet was resuspended overnight in 20 mM Tris at pH 7.0 and clarified at 4000*g* for 10 min. Virus was again pelleted at 61 000*g* and resuspended in a minimal amount of 20 mM Tris at pH 7.0 before clarifying by centrifugation for 10 min at 4000*g*.

TAV solutions were concentrated to about 14 mg/ml before crystallization at 18 °C and pH 8.5 using 14–17% ethanol and 100 mM Tris as previously reported by Canady et al. (1995). Crystals were grown by vapor diffusion using sitting drops in Cryschem plates (Hampton Research, Laguna Niguel, CA) sealed with clear plastic tape. Drops contained 10 μl of virus suspension mixed with 10 μl of precipitant in vapor equilibrium with 1 ml of precipitant in the reservoir. Crystals were visible after 1 week and grew to full size in about 2 weeks. Approximately 24 h prior to data collection, 10 μl of a solution containing 100 mM Tris (pH 8.5), 20% MPD, 10% ethanol, and 0.04% sodium azide was added to the crystal drops in order to reduce radiation damage during data collection.

2.2. Data collection and reduction

Data were collected at 25 °C at the National Synchrotron Light Source beamline X12B at Brookhaven National Laboratory, and at the Stanford Synchrotron Radiation Laboratory beamline 7-1 using oscillation angles of 0.5 °. Two hundred thirty-nine images from 33 crystals were processed using DENZO and SCALEPACK (Otwinowski and Minor, 1997). Spot mosaicities ranged from 0.15 to 0.35. Crystals belong to space group I222 with cell dimensions of $\mathbf{a} = 294.3\,\text{Å}$, $\mathbf{b} = 327.4\,\text{Å}$, $\mathbf{c} = 382.1\,\text{Å}$. A total of 1444 765 independent observations were reduced to 156 468 unique reflections that were used in refinement. Data had an overall $R_{\text{sym}} = 0.230$ for all data to 3.4 Å and was 62% complete. Using the formula of (Weiss, 2001) based on the completeness and maximum resolution of the data, the effective resolution is 4 Å.

2.3. Structure solution and refinement

Space group constraints demand that the virus particle be centered at the origin with three mutually perpendicular icosahedral twofold axes coincident with the unit cell axes. This implies that the particle has one of two possible orientations related to each other by a rotation of 90 ° about any of the cell axes. Self-rotation searches for fivefold and threefold axes identified the correct orientation. Phase extension using a CCMV model was unsatisfactory compared to direct molecular replacement using a model of CCMV mutated to the TAV sequence according to the alignment of Wikoff et al. (1997). This model was positioned at the origin of the unit cell in the proper orientation. Incremental radial expansion of the model produced a maximum in the correlation coefficient of 0.175 for 5–15 Å data with an outward radial displacement of 7 Å. Subsequent rigid body refinement and conjugate gradient minimization produced an R factor of 0.453. Iterative model rebuilding to NCS averaged maps and refinement failed to reduce the R factor below 0.34. At this point, Dr. Tom Smith at Purdue University generously provided a model for CMV, which was superimposed on the best model to this point. The R factor was immediately reduced to 0.27. This model was then mutated to the TAV sequence. Iterative model rebuilding and Powell minimization produced the model presented here. In addition to NCS constraints based on the icosahedral symmetry of the particle, NCS restraints between subunits were employed in the latter stages of refinement for all β-strands and troublesome α-helices. Without these restraints, the secondary structural elements between the different subunits showed poor consistency.

Table 1
Refinement results and model geometry

R_{free} $F > 2\sigma$ in bold											
Resolution		No. reflections		R value		Accum.		% Completeness		% Accum.	
7.32	100.00	1212	**1114**	0.196	**0.176**	0.196	**0.176**	4.7	**4.3**	4.7	**4.3**
5.81	7.32	1167	**1031**	0.226	**0.199**	0.206	**0.184**	4.6	**4.1**	4.7	**4.2**
5.08	5.81	1190	**977**	0.267	**0.215**	0.222	**0.192**	4.7	**3.9**	4.7	**4.1**
4.61	5.08	1215	**978**	0.275	**0.211**	0.233	**0.196**	4.9	**3.9**	4.7	**4.1**
4.28	4.61	1152	**826**	0.342	**0.239**	0.250	**0.202**	4.6	**3.3**	4.7	**3.9**
4.03	4.28	1153	**718**	0.453	**0.294**	0.273	**0.212**	4.6	**2.9**	4.7	**3.7**
3.83	4.03	479	**430**	0.423	**0.389**	0.281	**0.222**	1.9	**1.7**	4.3	**3.4**
3.66	3.83	220	**220**	0.382	**0.379**	0.284	**0.226**	0.9	**0.9**	3.9	**3.1**
3.52	3.66	67	**67**	0.386	**0.386**	0.285	**0.227**	0.3	**0.3**	3.5	**2.8**
3.40	3.52	30	**30**	0.491	**0.488**	0.285	**0.228**	0.1	**0.1**	3.1	**2.5**
R_{work} $F > \sigma$ in bold											
7.32	100.00	22858	**21452**	0.189	**0.173**	0.189	**0.173**	88.8	**83.3**	88.8	**83.3**
5.81	7.32	22401	**19479**	0.226	**0.192**	0.202	**0.179**	88.7	**77.2**	88.8	**80.3**
5.08	5.81	22231	**18293**	0.253	**0.200**	0.215	**0.185**	88.5	**72.8**	88.7	**77.8**
4.61	5.08	22105	**17568**	0.273	**0.205**	0.227	**0.189**	88.3	**70.2**	88.6	**75.9**
4.28	4.61	22337	**16574**	0.324	**0.232**	0.243	**0.196**	89.2	**66.2**	88.7	**74.0**
4.03	4.28	22705	**14461**	0.438	**0.283**	0.266	**0.205**	90.9	**57.9**	89.1	**71.3**
3.83	4.03	8254	**7529**	0.377	**0.347**	0.272	**0.213**	33.1	**30.2**	81.1	**65.5**
3.66	3.83	3713	**3711**	0.371	**0.366**	0.274	**0.216**	14.9	**14.9**	72.9	**59.2**
3.52	3.66	1372	**1371**	0.364	**0.359**	0.275	**0.217**	5.5	**5.5**	65.5	**53.3**
3.40	3.52	607	**607**	0.409	**0.402**	0.275	**0.218**	2.4	**2.4**	59.2	**48.2**
3.4	100	156468	**127436**	0.275	**0.218**	0.275	**0.218**	62.4	**50.8**	62.4	**50.8**

RMSD	B_{factor} statistics (Å^2)				Ramachandran statistics	No. of residues	
	Molecule	All	Main chain	Side chain			
Bonds = 0.009 Å					Most favored regions	317	66.5%
Angles = 1.66°	A	107.3	105.4	109.3	Additional allowed regions	147	30.8%
Dihedral = 29.3°	B	97.6	94.2	101.1	Generously allowed regions	10	2.1%
Improper = 1.03°	C	103.2	100.8	105.8	Dissallowed regions	3	0.6%

The R factor for the final model is 0.218 for 127 436 reflections with $F \geqslant 2\sigma$; other statistics related to refinement and model quality are given in Table 1.

Diffraction patterns from crystals of TAV are strong to approximately 4 Å but decline rapidly beyond that limit with low completeness in high-resolution shells. Fortunately, however, there is 15-fold redundancy in the crystallographic asymmetric unit. It is this high redundancy in reciprocal, as well as real space, that makes it possible to solve the structures of viruses at relatively low resolutions, as has been done, for example, in the cases of alfalfa mosaic virus (Kumar et al., 1997), physalis mottle virus (Krishna et al., 1999), and murine polyomavirus (Stehle and Harrison, 1996).

Furthermore, this high redundancy for icosahedral viruses also explains why the R_{free} and conventional R factors tend to converge to the same value, since NCS-related reflections are in the working and test datasets. This is seen here for TAV where $R_{free} = 0.228$ and $R = 0.218$. The R_{free} for virus structures, therefore, does not have the same utility as for conventional structures; on the other hand, a failure to converge to R would surely suggest some difficulty with the refinement.

2.4. Procedures and programs

Fifteen noncrystallographic symmetry operators were determined for the particle orientation and the placement of the ABC trimer in the capsid. These NCS operators were used throughout refinement and in the averaging of electron density maps. XPLOR 3.851 (Brünger, 1991, 1992; Brünger et al., 1987) performed simulated annealing and conjugate gradient minimization. PROCHECK (Laskowski et al., 1993) was used to evaluate model quality. Initially, XPLOR was used to calculate electron density maps, which were then NCS-averaged with RAVE (Jones, 1992) using masks generated with the program MAMA (Kleywegt and Jones, 1994). Later, CNS (Brünger et al., 1998) was used with more facility to generate NCS-averaged maps; however, MAMA masks, encompassing the protein shell and the entire particle interior, were retained for averaging. The program O (Jones and Kjeldgaard, 1994) was used for manual rebuilding. Images of surfaces were created with the programs GRASP (Nicholls et al., 1991) and Insight 2000 {from Accelrys: http://www.accelrys.com} with charge assignments on normally ionizable residues. Ribbon models were made using the Molray interface to

Persistence of Vision Ray Tracer (POV-Ray) and Molscript (Kraulis, 1991), with rendering performed by Raster3d (Merritt and Bacon, 1997). Minimaps were prepared with the Xcontur program in XtalView (McRee, 1999). Contacting surface areas were calculated in XPLOR with the algorithm of Lee and Richards (1971) using a probe radius of 1.4 Å.

3. Results and discussion

The asymmetric unit of the I222 crystals used in the X-ray analysis of the TAV structure is equivalent to one-quarter of the virion and comprises 15 triangular faces each composed of the three icosahedrally distinct protein subunits A, B, and C. All have identical amino-acid sequences but assume three slightly different subunit conformations to accommodate their structural roles in the virion. Therefore, 15-fold noncrystallographic symmetry (NCS) was used in all averaging operations and throughout refinement. In order to maintain structural consistency, NCS restraints among A, B, and C subunits for β-strands and helices were employed. In the final model of TAV, the pentameric A subunits included residues 44–217, while the B and C subunits, comprising the hexameric capsomeres, included amino acids 36–217 and 34–217, respectively. The coat protein exhibits the canonical "jelly roll" β-barrel domain, but connected through hinge polypeptides to helices, which form amphipathic clusters interior to each capsomere (see Fig. 1). Distal amino-terminal segments of the three subunits were not visible in electron density maps.

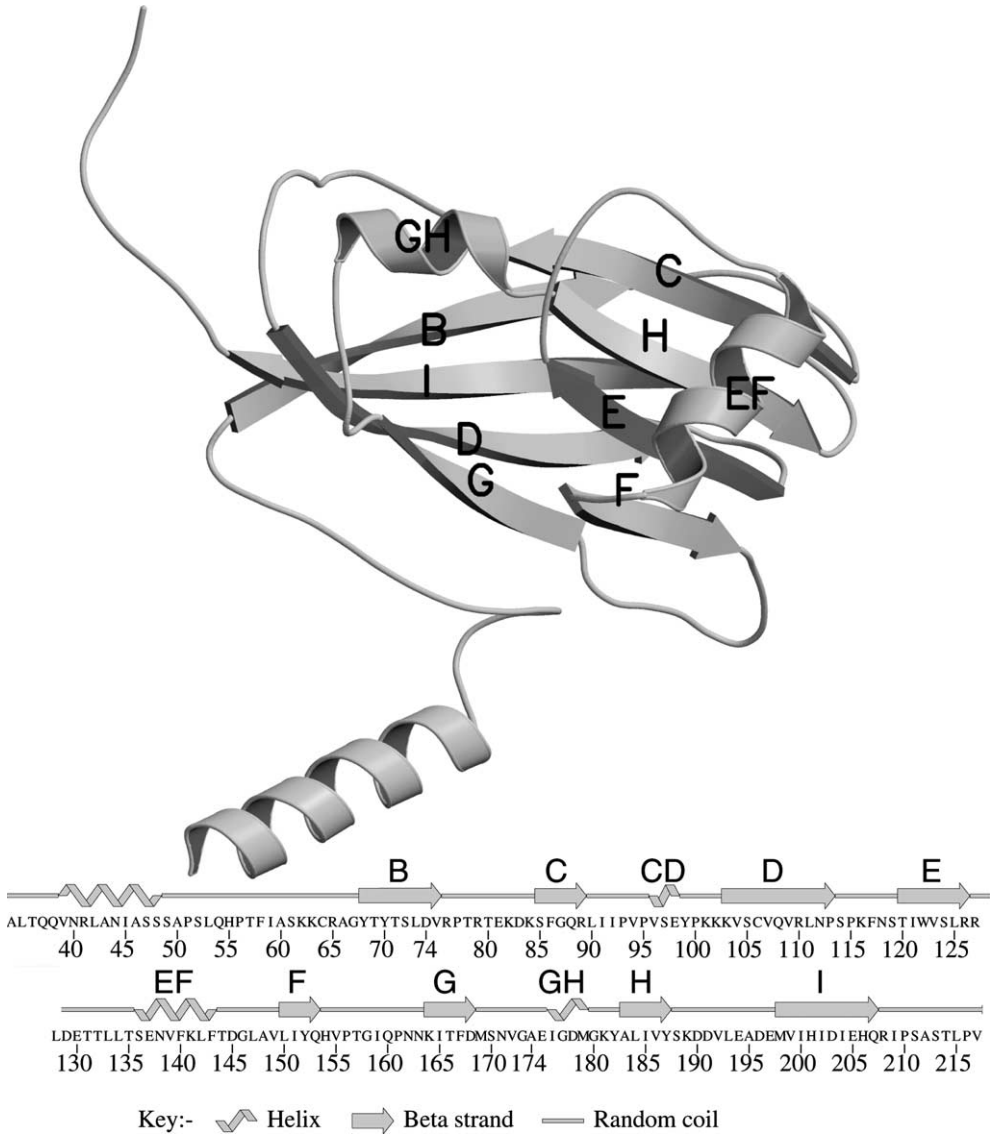

Fig. 1. Ribbon image of the C subunit of TAV with sheets and helices of interest labeled. At the bottom of the figure is a secondary structure diagram with numbering and one-letter amino-acid abbreviations.

The final TAV model also includes putative Mg^{2+}ions on the quasi-threefold axes relating A, B, and C subunits. An additional ion of ambiguous character was also observed on the fivefold axis, but well in the virion interior; this was modeled as a putative phosphate ion.

The protein subunits are shown as they are assembled to make hexameric capsomeres (from B and C subunits), pentameric capsomeres (from A subunits), and distributed about the quasi-threefold axis (A, B, and C subunits) in Fig. 2. As with CMV, there are no β-annuli as seen in viruses from some other families (Johnson and Rueckert, 1997; Larson et al., 2000).

There are deep indentations in both the pentameric and hexameric capsomeres, which would otherwise result in channels leading to the virion interior. The pores, however, are completely obstructed by the helices clustered about the fivefold and sixfold axes. Interactions among subunits within capsomeres, both pentameric and hexameric, are extensive, with fewer contacts between the capsomeres. The fewest interactions are among A, B, and C subunits at the quasi-threefold axes.

The appearance of the intact virion is seen in Fig. 3 along with relevant dimensions. A thin cross section passing through the center of the capsid and containing fivefold and quasi-sixfold axes is also shown. In Fig. 4,

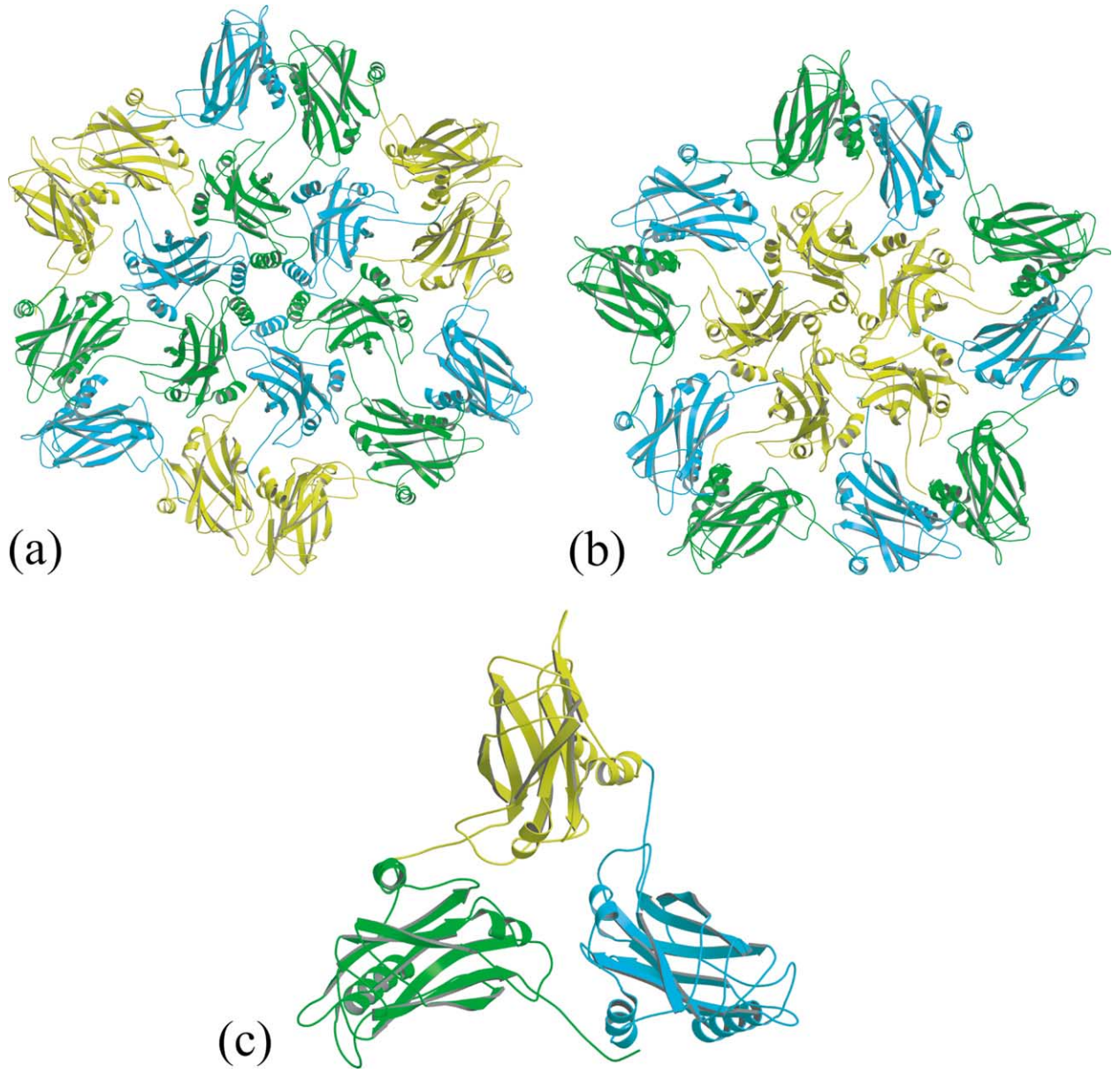

Fig. 2. Ribbon diagrams of the polypeptide backbones of TAV capsid protein subunits forming (a) hexameric capsomeres, (b) pentameric capsomeres, and (c) the trimer of A, B, and C subunits formed about a quasi-threefold axis. A subunits are yellow, B subunits are cyan, and C subunits are green.

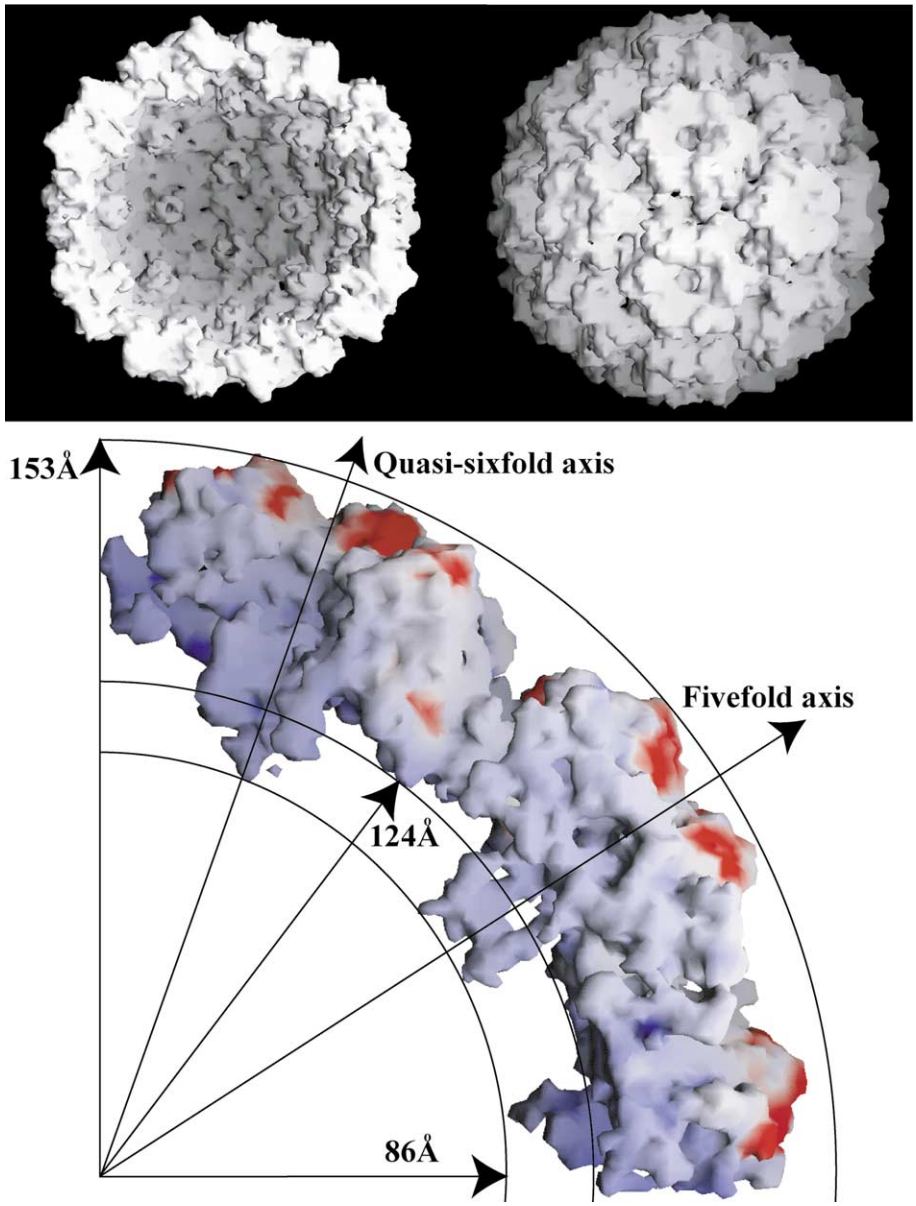

Fig. 3. At top are the accessible surface areas of the interior and exterior of the TAV model. Below is a quarter cross section approximately 40 Å thick of TAV, which contains a fivefold and quasi-sixfold axis. As indicated, the maximum particle radius is 153 Å. The minimum radius of the interior of the capsid, without the N-terminal helices, is 124 Å, and is 86 Å with those helices included.

the interior and exterior surfaces are colored according to electrostatic potential, with positive colored blue and negative colored red. As one might expect, the interior surface of TAV, even without the full-length positively charged N-termini, has a predominantly positive potential, suggesting a close electrostatic association between the interior of the protein capsid and the negatively charged genomic RNA.

3.1. Comparison of TAV with CMV

Detailed comparisons of important features for TAV and CMV (PDB code 1F15) are discussed more fully below, but some points are appropriate here. The Blencowe strain of TAV used in this study contains 217 amino-acid residues while the FNY strain of CMV solved by Smith et al. (2000) has 218. This results from a single deletion in TAV corresponding to serine 148 in CMV. Serine 148 occurs in the EF loop[2] region connecting two strands of the β-barrel, and its deletion probably has little effect on the overall loop structure. In fact, the *pepper isolate* of TAV does not have this deletion, further suggesting its lack of structural significance. The region extending from about positions

[2] Strand, loop, and helix letter designations are according to Smith et al. (2000).

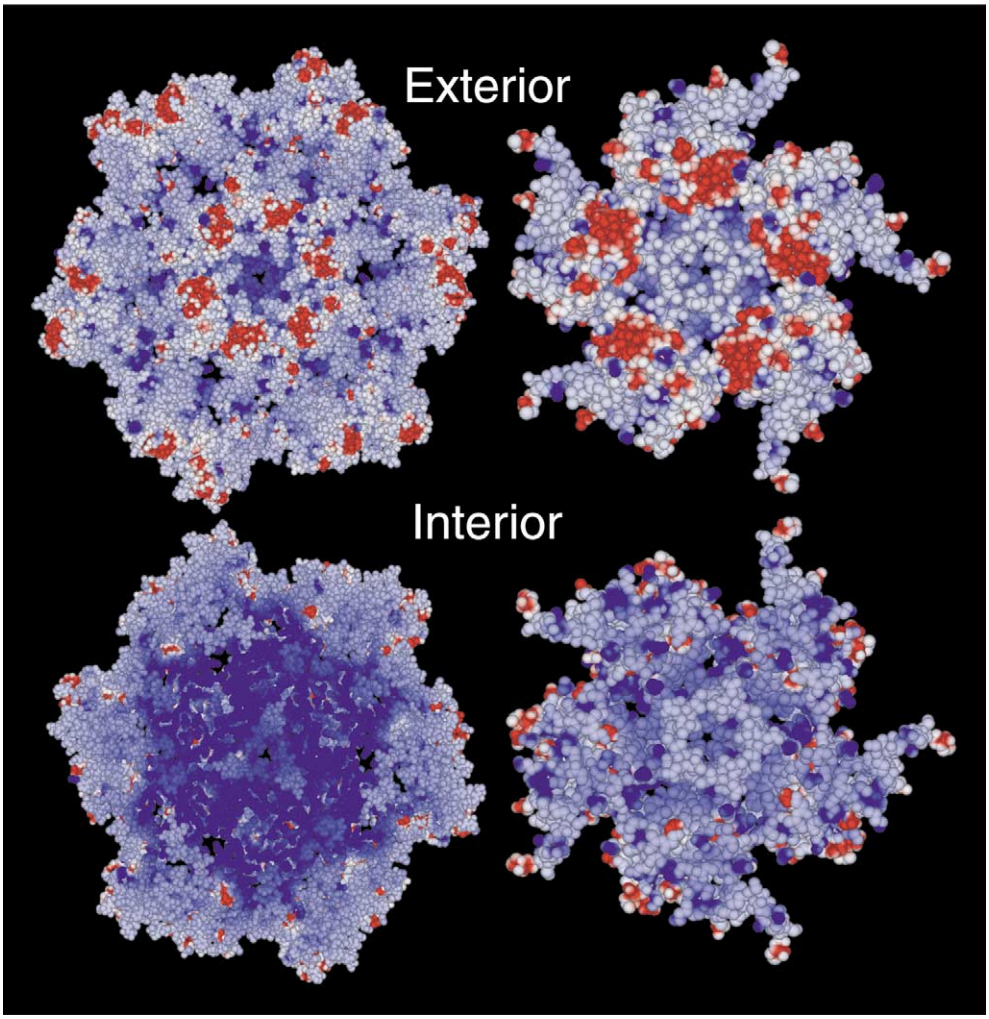

Fig. 4. Van der Waals surface representations of the hexameric (left) and pentameric (right) capsomeres of TAV with negative potential colored red and positive potential colored blue. Although the overall electrostatic potential on the exterior is predominantly positive, carboxyl groups provided by acidic residues in the FG loops produce distinctive negatively charged rings on the cusps of both types of capsomeres. The interior surfaces of the capsomeres are very positive and, therefore, electrostatically complementary to the negatively charged, encapsidated RNA.

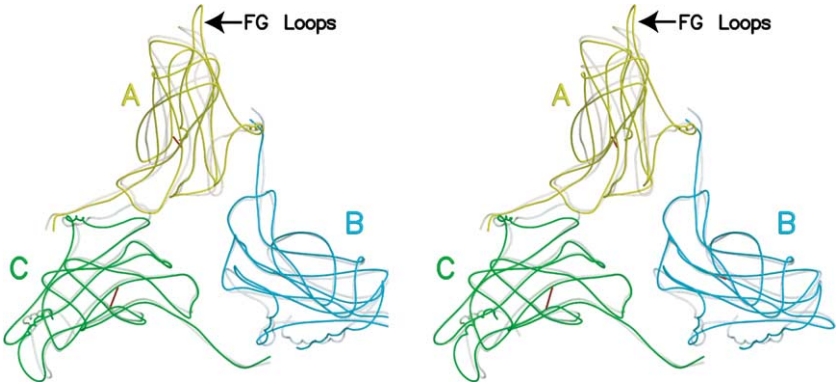

Fig. 5. A stereo view of the ABC trimer of TAV superimposed on the corresponding subunits of CMV. The A, B, and C subunits of TAV are shown in yellow, cyan, and green, respectively. The CMV subunits are colored gray. As is evident here, most of the major differences in the courses of the polypeptide chains are found in the loop regions connecting strands of the "Swiss roll" β-barrels. The disulfide bonds in TAV are shown in red.

129 to 148 in all three subunits is that of greatest structural difference between the backbones of TAV and CMV.

The backbone atoms in this region have RMSDs nearly five times the overall average when TAV is compared with CMV. These lead to subtle variations

along the EF loop which cause a relative shift of the EF α-helix. Amino acids 129 and 148, the bounding residues of this variable region, are prolines in CMV but glutamate and alanine, respectively, in TAV. The dissimilarity of the sequences at these two positions, in conjunction with the inherent flexibility of the loop region itself, is likely a major contributor to these observed conformational differences. These residues are exposed to the exterior environment of the virus and could help confer host specificity or transmission characteristics unique to each virus.

The A, B, and C subunits of TAV are seen in Fig. 5 superimposed on the corresponding polypeptides of CMV. The RMSDs for the α-carbons of the three subunits in TAV with their corresponding subunit in CMV are 2.15 Å for A, 1.89 Å for B, and 1.86 Å for C subunits. These may be compared with the RMSDs for the A, B, and C subunits within TAV which are 1.40 Å for AB, 1.46 Å for AC, and 1.20 Å for BC subunits. Thus, there is a somewhat greater difference between the main chain conformations of corresponding TAV and CMV subunits than among the A, B, and C subunits of TAV.

The crystals used for analysis of CMV were grown at low pH where carboxyl groups tended to be more protonated, and no metal ions were observed in the X-ray structure. The TAV crystals, on the other hand, were grown at pH 8.5; thus, all carboxyl groups were negatively charged, and putative Mg^{2+} ions were observed at quasi-threefold axes. The prominent amino-terminal helices of the hexameric capsomeres seen in CMV are also present in TAV, but additional density is seen in TAV for the upper portions of helices clustered about the fivefold axes as well.

Overall, the appearances of the two viruses, TAV and CMV, are very similar, with subunit interactions more or less the same. A detailed comparison of these might be ill advised given the modest resolution of the TAV model. Fig. 6, however, provides a measure of the calculated contact areas between subunits for TAV and CMV.

3.2. N-terminal helices

TAV, like CMV, has six amphipathic helices formed by the amino-terminal domains of the B (residues 36–49) and C (residues 34–49) subunits directed into the interior of the virion (to a distance of about 90 Å from its center), and assembled as bundles about each threefold (quasi-sixfold) icosahedral axis. These are illustrated in Fig. 7a. The residues preceding these helices (i.e., residues 1–35 and 1–33 in subunits B and C, respectively) are disordered and not visible in electron density maps. The corresponding helices in the CMV model (Smith et al., 2000) consist of residues 29–48 and 28–48 of subunits B and C, respectively, and extend into the interior

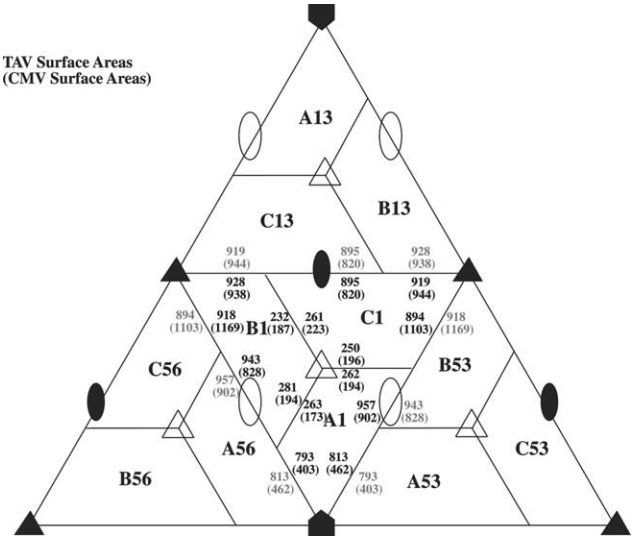

Fig. 6. A schematic diagram of the TAV capsid showing contacting surface areas for symmetry-related protein subunits. Numbers in parentheses are the corresponding values for CMV. Along each unique interface, the surface area buried by that interface is noted; symmetry related interfaces are shown in light gray. This provides some measure of the degree of interaction of the two subunits across each interface. Exact and quasi-rotation axes are identified by solid symbols and open symbols, respectively.

to a radius of 86 Å. The increased length of the helices and the lower thermal parameters suggest a more ordered assembly exists in CMV.

In the CMV maps amphipathic helices were observed only for the B and C subunits around the quasi-sixfold but not for the pentameric A subunits. In TAV, however, this is not the case. In electron density maps of TAV (Fig. 7b), the upper portions of α-helices, including residues 44–49, are present for the A subunits, but the density diminishes before residue 44. This explains the differences in buried surface area between TAV and CMV for the A subunits as shown in Fig. 6. This observation suggests that groupings of five A subunit helices are indeed present about the fivefold axes (and probably in CMV as well), but that the fivefold arrangement is less stable or more dispersed than the six-helix bundle. This results in a somewhat higher degree of disorder of the individual helices. The secondary structure of the amino-terminal helix domains of the A subunits may be the same as those of the B and C subunits but less distinct due to the increased disorder. It is also possible that the A subunits have shorter helices than the B and C subunits with some nonhelical and disordered structure before residue 44.

The amphipathic α-helices surrounding both the three- and fivefold icosahedral axes are joined to the β-barrels of the capsid proteins, as shown in Fig. 7c, by extended polypeptides about 17 Å in length composed of the six-amino-acid segment from proline 51 to proline 56. This polypeptide is less well ordered in the A

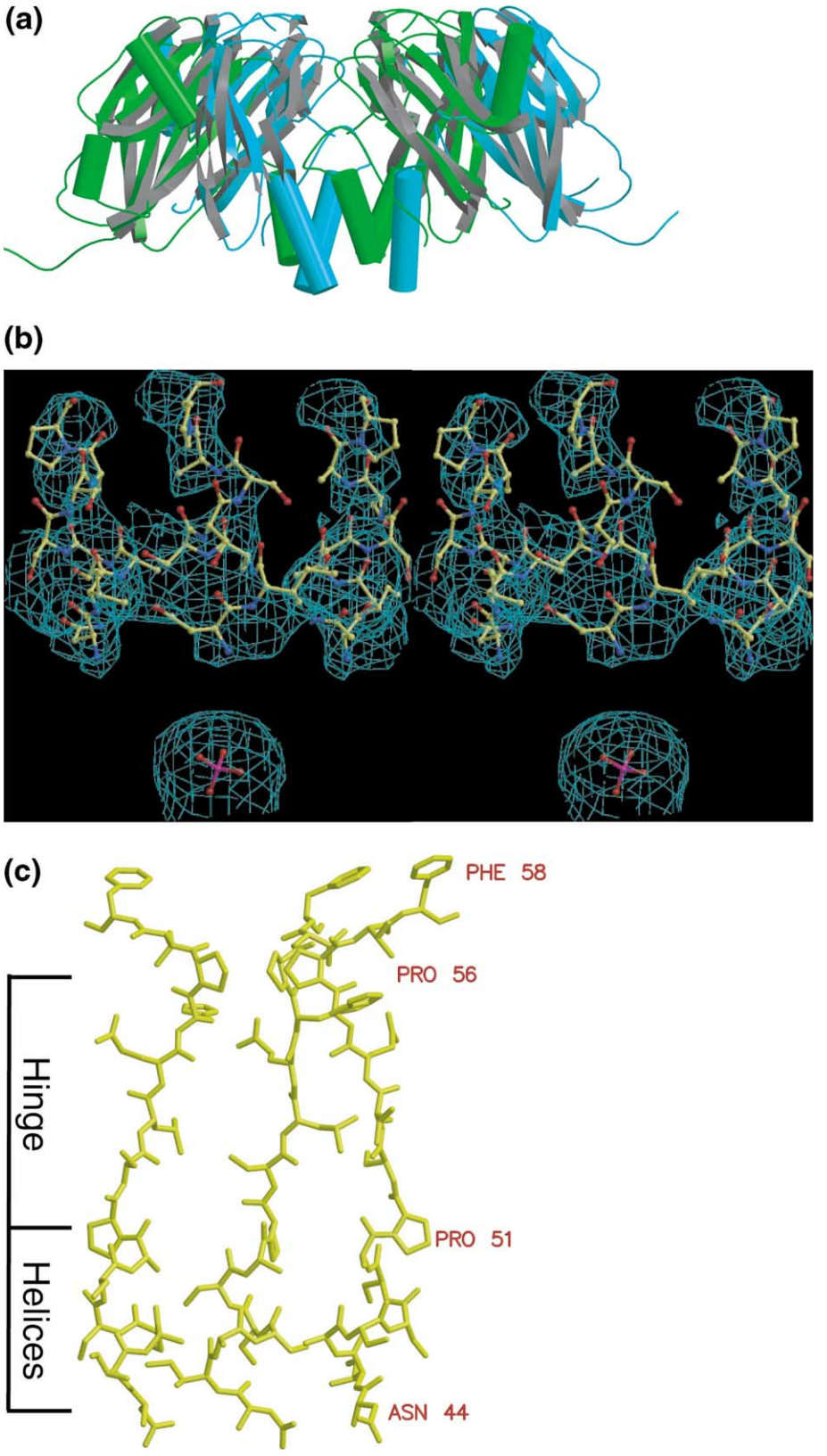

Fig. 7. In (a) are the B (cyan) and C (green) subunits of TAV organized about the quasi-sixfold axis (exact threefold axis) to form a hexameric capsomere. The figure has been slabbed around the helix bundle for clarity. The α-helices are represented as cylinders and the β-strands as ribbons. The six amino-terminal α-helices form a distinctive cluster that protrudes at least 20 Å into the interior of the virion. In (b) is illustrated the N-terminal helices of the A subunits superimposed on the density of a $2F_o–F_c$ map contoured at 0.4σ. Also shown is the density of the putative phosphate ion on the fivefold axis. The helices are joined to the β-barrels of each subunit by hinge polypeptides, three of which are illustrated in (c).

subunits than in the B and C subunits in TAV, and it is apparently completely disordered in CMV. It is almost certainly the conformational flexibility of this polypeptide link that confers the mobility and freedom the α-helices require to form both fivefold and sixfold arrangements. In this sense, it acts as a hinge region, a feature commonly seen joining domains in larger proteins. In fact, the helices have slightly different orientations with respect to the β-barrels between hexamers and pentamers due to changes in the hinge region resulting from the structural differences between the fivefold and sixfold capsomeres.

3.3. Ion-binding sites

The ABC trimer (shown in Fig. 2c) possesses a quasi-threefold axis through its center. The side chains of the three quasi-symmetric glutamate 175 residues are directed toward this axis. $2F_o$–F_c composite omit electron density maps, contoured at the 3-sigma level, consistently exhibited density at the center of this carboxylate triangle suggesting the presence of a cation. This was modeled as a putative Mg^{2+} ion as illustrated in Fig. 8, but could be Ca^{2+} or some other cation. While no magnesium was intentionally added during purification or crystallization, there is biochemical evidence that supports the binding of Mg^{2+} ions by TAV (Habili and Francki, 1974b; Savithri et al., 1984). Distances between the putative Mg^{2+} ion and the carboxylate oxygen atoms range from 3.5 to 4.2 Å, which suggests that the cation is hydrated and that water molecules bridge between the cation and the glu175 carboxyl groups. Indeed, at low contour levels the side chain density merges with that of the ion, supporting this idea. Furthermore, in brome mosaic virus (BMV) a Mg^{2+} ion was observed at a similar position on the quasi-threefold axis, coordinated by three glutamate side chains with magnesium to oxygen distances of about 2.6 Å (Lucas et al., 2001). Unlike BMV, however, the ion in TAV is much further away from the coordinating side chains and is less likely to significantly contribute to particle stability. Indeed, this would help to explain the lack of pronounced swelling of TAV at high pH in the presence of cations.

Another consistently observed feature in $2F_o$–F_c electron density maps was a peak (at the 2-sigma level) on the fivefold axis, approximately 10 Å from the first modeled residue (residue 44) of the N-terminal helix of the A subunit (see Fig. 7b). The proximity of this peak to the five-helix bundle suggests some type of association between them. There are several possible explanations for this peak. One is that this point is simply the confluence of otherwise disordered viral components (whether protein from the nonmodeled N-termini of the A subunits or RNA) whose common presence appears as density representing nearly fully occupied space. Another possibility is the presence of an ion, and, thus, we have modeled it as a phosphate ion.

3.4. Disulfide bond

In the 217 amino-acid sequence of TAV, there are two cysteine residues, one immediately before β-strand B (cys64), and a second (cys106) in β-strand D. Cys106 occupies the position of a conserved arginine residue in other members of the bromoviridae family such as CMV and peanut stunt virus of the cucumoviruses, and CCMV and BMV of the bromoviruses (Wikoff et al., 1997). The two internal cysteine residues form a disulfide bond, a linkage not previously observed in other wild-type bromoviridae. This bond is illustrated in Fig. 9 superimposed on electron density of a $2F_o$–F_c map. The disulfide bond length is 2 Å. The disulfide bridges are on the inside of the capsid at the opposite ends of the β-sheets from the salt bridge networks (described below) on the exterior. Both could provide mechanisms for enhancing β-sheet stability.

The only other reported occurrence of a disulfide bridge was also in a bromovirus, a CCMV mutant isolated by Bancroft et al. (1971). That disulfide bond was the result of a single point mutation of C to U at position 1435 of RNA3 (or 86 of RNA4), which caused replacement of arg26 by cysteine. The resulting disulfide bridge was located at the base of the CCMV β-annulus.

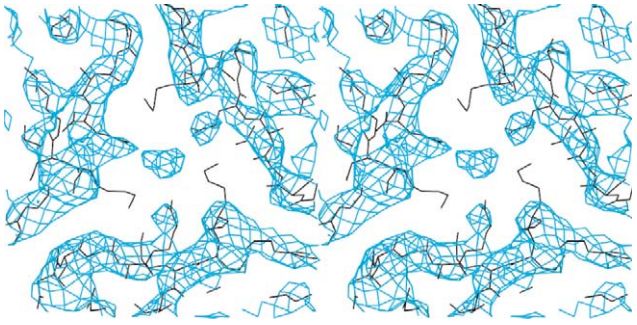

Fig. 8. At the quasi-threefold axis, three quasi-symmetrical glu175 side chains extending from each subunit of the ABC trimer surround density representing the putative Mg^{2+} ion. The density is from a $2F_o$–F_c composite omit map contoured at 1σ.

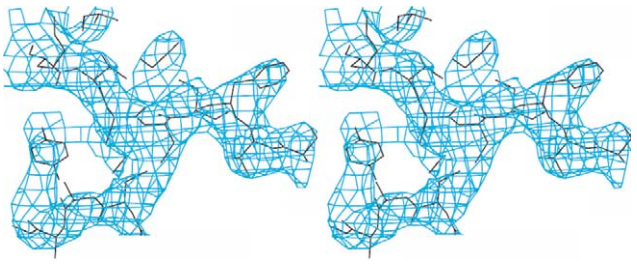

Fig. 9. A stereo diagram of the disulfide bond in the TAV C subunit superimposed on $2F_o$–F_c electron density contoured at 1.6σ.

In a nonreducing environment, it allowed the virus particles to swell without loss of integrity under conditions that completely destabilize the wild-type virus (Fox et al., 1996).

3.5. Salt effects on TAV

Cucumoviruses can be disassembled in concentrated salt solutions such as 1.5 M KCl or 1 M $CaCl_2$, and its protein will reassemble into infectious, wild-type particles upon return to physiological conditions. It will not reassemble, however, if no RNA is present, from either TAV itself or from some heterologous source. Other quasi-nucleic acids, small oligonucleotides, or DNA can also be encapsidated at low efficiency; thus, there appears to be rather little specificity involved (Kaper, 1975).

TAV apparently exists, more or less permanently, in a state equivalent to the "swollen state" of BMV. However, it does not undergo a pH-dependent swelling, as BMV does (Kaper, 1975). The capsid appears to be rather loosely constructed, in comparison with other icosahedral plant viruses, with relatively few interactions among subunits. The assembly and the maintenance of the native virion appear to be very much dependent on protein–RNA interactions. The capsid structure is sufficiently open that the encapsidated RNA can be directly degraded by RNase even in the native state (Habili and Francki, 1974b; Kaper, 1975).

3.6. RNA

Density consistent with three-nucleotide segments of single-stranded RNA was identified in close proximity to the interior of the capsid at the quasi-twofold axes relating A and B subunits (Fig. 10). By symmetry, this would account for 180 nucleotides within the virion. Interacting with each RNA segment, which is in an approximately helical conformation with stacked bases, are the side chains of ser211, arg208, and arg65 of the A subunit and arg208 of the B subunit. It has been shown that nucleic acids, or at least oligonucleotides, are necessary for assembly to proceed (Habili and Francki, 1974a; Kaper, 1975). The positioning of the ordered nucleic acid at the AB interface suggests a role in directing capsid assembly and maintaining virion stability.

3.7. FG loops

The FG loops of each monomer form the wall of the pore exterior to the N-terminal helices at both the fivefold and quasi-sixfold axes in both CMV and TAV. At the fivefold axes in CMV, the FG loops of the A subunits are drawn away from the pore compared to the FG loops at the quasi-sixfold axes, making the former slightly larger than the latter. In TAV, however, the FG loop is closer to the center of the pore at the fivefold axis with the backbone shifted about 3.3 Å inward compared to its position in the hexameric capsomere. This change in pore dimensions determines accessibility of the top of the N-terminal helices to the exterior environment of the virus. This may in turn affect the RNase sensitivity of the intact virus. The relatively smaller pore size at the fivefold axes of TAV may explain the greater resistance to RNase of TAV compared with CMV (Habili and Francki, 1974a,b).

3.8. Salt bridges

With most $T = 3$ icosahedral plant viruses, the outermost rim of the pentameric and hexameric capsomeres are formed by the BC, HI, and DE β-loops with the FG

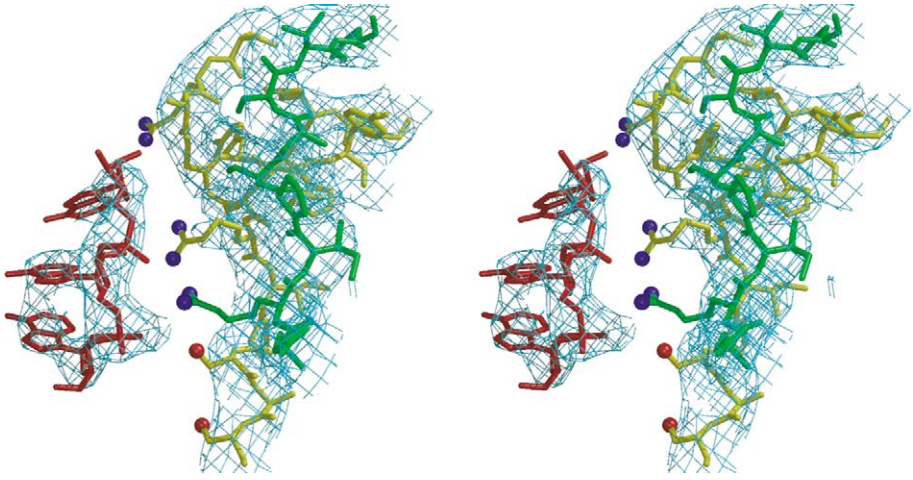

Fig. 10. A stereo diagram of an RNA trinucleotide segment, observed on the interior of the TAV capsid near a quasi-twofold axis, is shown in red. The probable amino-acid residues, which interact with the RNA phosphate backbone, are illustrated as well. These residues are (from top to bottom): arg65, arg208 of the A subunit; arg208 of the B subunit; and ser211 and ser213 of the A subunit.

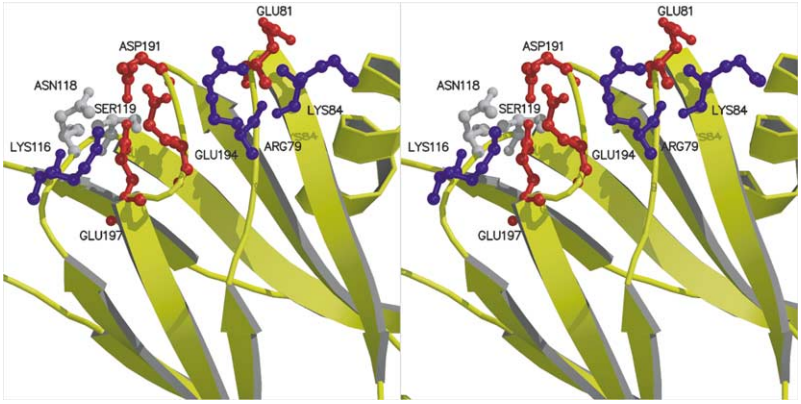

Fig. 11. A stereo diagram showing the charged residues making up the salt bridge networks at the exterior ends of the β-barrels. Negatively charged groups are in red and positively charged groups are in blue. The network may contribute to the stabilization of the β-barrels, as well as provide some electrostatic recognition site.

β-loops defining the pore sizes at the five- and sixfold axes. In TAV, as well as CMV, there is a concentration of charged residues in these loops. In the HI loop of both, there are five negative residues (asp 190, asp191, glu194, asp196, and glu197) and one positive residue (lys189). The charged residues in the BC and DE loops are not well conserved between TAV and CMV. The BC loop in TAV contains three positive residues (arg79, lys82, and lys84) and two negative residues (glu81 and asp83). The corresponding residues in CMV are lys79, arg82, ser84, asp81, and gly83, with only one negative and two positive residues. The DE loops of both TAV and CMV have a lysine at residue 116 but differ at residue 118 where TAV has an asparagine residue versus an aspartic acid in CMV. Disposition of the charged residues in this region for TAV are illustrated in Fig. 11.

It has been suggested (Smith et al., 2000; Speir et al., 1995) that this region may serve an ion-binding function. Ions, however, were not observed in either CCMV or CMV, although it was argued that this could have been a consequence of crystallization conditions, specifically the presence of EDTA in cowpea chlorotic mottle virus (CCMV) mother liquors, and low pH in the case of CMV. TAV, however, was crystallized at pH 8.5 and in the absence of EDTA. Furthermore, the presence of a putative cation at the quasi-threefold axis suggests that purification and crystallization conditions were sufficiently tolerant to leave bound ions intact. Rather than forming an ion-binding site, the negatively charged residues may be components of a more extensive network of salt linkages that tie these loops together through bridging between glu194 and arg79, lys116 and glu197, lys82 and asp191. Intraloop salt bridges may also form between glu81 and arg79, or lys84, or both (see Fig. 11). At an effective resolution of about 4 Å, the positions of some of these side chains are ill defined, but nonetheless consistent with such an arrangement.

As seen in Fig. 4, these networks of residues produce the only negatively charged areas on the exterior surface of TAV virions. These negative clusters, present at the outermost rims of the capsomeres, would almost certainly be the first points of contact with foreign surfaces. This may have implications in regards to both viral transmission and cell infection. CMV is transmitted by aphids through attachment of the virus to aphid mouthparts, followed by plant infection through egestion. The HI loop residues are essential for this process (Smith et al., 2000). Infection of individual cells may occur by a similar process in which complementary, positively charged regions on the exterior of target cells serve as binding sites for the virions.

There appear to be three intersubunit salt bridges in the ABC trimer of the CMV structure from residue lys101 to asp179, lys182 to asp100, and lys127 to asp100. Only the first of these salt bridges is retained in TAV (lys101 to asp178 in TAV numbering). Asp100 of CMV corresponds to pro 100 in TAV, preventing the same salt bridge network that exists in CMV. Arg127 in TAV partially compensates for this loss by forming a salt bridge with glu98. The putative magnesium ion bound at the quasi-threefold may also help compensate for the loss of the other salt bridges. The possibility of trimer stabilization by cation binding at the quasi-threefold in the CMV structure is diminished by the shorter side chains of asp176 as compared to the corresponding glu175 in TAV.

3.9. Coordinates

The coordinates have been deposited in the RCSB Protein Data Bank as entry 1LAJ.

Acknowledgments

The authors are grateful to Dr. Tom Smith for supplying the CMV coordinates. Data were collected at the National Synchrotron Light Source, Brookhaven

National Laboratory, which is supported by the US Department of Energy, Division of Materials Sciences, and Division of Chemical Sciences. This research was supported by grants from the NIH and NASA. Portions of this research were also carried out at the Stanford Synchrotron Radiation Laboratory, a national user facility operated by Stanford University on behalf of the US Department of Energy, Office of Basic Energy Sciences. The SSRL Structural Molecular Biology Program is supported by the Department of Energy, Office of Biological, and Environmental Research, and by the National Institutes of Health, National Center for Research Resources, Biomedical Technology Program, and the National Institute of General Medical Sciences.

References

Bancroft, J., McLean, G., Rees, M., Short, M., 1971. The effect of an arginyl to a cysteinyl replacement on the uncoating behavior of a spherical plant virus. Virology 45, 707–715.

Brünger, A.T., 1991. Simulated annealing in crystallography. Annu. Rev. Phys. Chem. 42, 197–223.

Brünger, A.T., 1992. The free *R* value: a novel statistical quantity for assessing the accuracy of crystal structures. Nature 355, 427–474.

Brünger, A.T., Kuriyan, J., Karplus, M., 1987. Crystallographic *R* factor refinement by molecular dynamics. Science 235, 458–460.

Brünger, A.T., Adams, P.D., Clore, G.M., DeLano, W.L., Gros, P., Grosse-Kunstleve, R.W., Jiang, J.-S., Kuszewski, J., Nilges, M., Pannu, N.S., Read, R.J., Rice, L.M., Simonson, T., Warren, G.L., 1998. Crystallography and NMR system: a new software suite for macromolecular structure determination. Acta Crystallogr. Sect. D 54, 905–921.

Canady, M.A., Leja, C.A., Day, J., McPherson, A., 1995. Preliminary X-ray diffraction analysis of crystals of tomato aspermy virus (TAV). Proteins 21, 265–267.

Fox, J.M., Zhao, X., Speir, J.A., Young, M.J., 1996. Analysis of a salt stable mutant of cowpea chlorotic mottle virus. Virology 227, 229–233.

Habili, N., Francki, R.I., 1974a. Comparative studies on tomato aspermy and cucumber mosaic viruses. I. Physical and chemical properties. Virology 57, 392–401.

Habili, N., Francki, R.I., 1974b. Comparative studies on tomato aspermy and cucumber mosaic viruses. II. Virus stability. Virology 60, 29–36.

Hollings, M., Stone, O.M., 1971. Tomato aspermy virus. CMI/AAB descript. Plant Viruses 79, 1–3.

Johnson, J.E., Rueckert, R., 1997. Assembly of spherical viruses. In: Chiu, W., Burnett, R.M., Garcea, R.L. (Eds.), Structural Biology of Viruses. Oxford University Press, Oxford.

Jones, T.A., 1992. A, Yaap, Asap, @#*? A set of averaging programs. In: Dodson, E.J., Gover, S., Wolf, W. (Eds.), Molecular Replacement. SERC Daresbury Laboratory, Warrington, pp. 91–105.

Jones, T.A., Kjeldgaard, M., 1994. O—The Manual, Version 5.10, Uppsala University Press, Uppsala.

Kaper, J.M., 1975. In: The Chemical Basis of Virus Structure, Dissociation and Reassembly. North-Holland, Amsterdam, pp. 333–352.

Kleywegt, G.J., Jones, T.A., 1994. Halloween ... Masks and bones. In: Bailey, S., Hubbard, R., Waller, D. (Eds.), From First Map to Final Model. SERC Daresbury Laboratory, Warrington, pp. 59–66.

Kraulis, P.J., 1991. Molscript: a program to produce both detailed and schematic plots of protein structures. J. Appl. Crystallogr. 24, 946–950.

Krishna, S.S., Hiremath, C.N., Munshi, S.K., Prahadeeswaran, D., Sastri, M., Savithri, H.S., Murthy, M.R.N., 1999. Three-dimensional structure of physalis mottle virus: implications for the viral assembly. J. Mol. Biol. 289, 919–934.

Kumar, A., Reddy, V.S., Yusibov, V., Chipman, P.R., Hata, Y., Fita, I., Fukuyama, K., Rossmann, M.G., Loesch-Fries, L.S., Baker, T.S., Johnson, J.E., 1997. The structure of alfalfa mosaic virus capsid protein assembled as a $T = 1$ icosahedral particle at 4.0-Å resolution. J. Virol. 71, 7911–7916.

Larson, S.B., Day, J., Canady, M.A., Greenwood, A., McPherson, A., 2000. Refined structure of desmodium yellow mottle tymovirus at 2.7 Å resolution. J. Mol. Biol. 301, 625–642.

Laskowski, R.A., MacArthur, M.W., Moss, D.S., Thornton, J.M., 1993. Procheck: a program to check the stereochemical quality of protein structures. J. Appl. Crystallogr. 26, 283–291.

Lee, B., Richards, F.M., 1971. The interpretation of protein structures; estimation of static accessability. J. Mol. Biol. 55, 379–400.

Lot, H. et al., Contribution a l'etude du virus de la mosa que du concumbre (CMV). Ann. Phytopathol. 4, 25–38.

Lucas, R.W., Kuznetsov, Y.G., Larson, S.B., McPherson, A., 2001. Crystallization of brome mosaic virus (BMV) and $T = 1$ BMV particles following a structural transition. Virology 286, 290–303.

McRee, D.E., 1999. Xta1view/Xfit—A versatile program for manipulating atomic coordinates and electron density. J. Struct. Biol. 125, 156–165.

Merritt, E.A., Bacon, D.J., 1997. Raster3d: photorealistic molecular graphics. Methods Enzymol. 277, 505–524.

Nicholls, A., Sharp, K.A., Honig, B., 1991. Protein folding and association: insights from the interfacial and thermodynamic properties of hydrocarbons. Proteins 11, 281–296.

O'Reilly, D., Thomas, C.J., Coutts, R.H., 1994. Nucleotide sequence of RNA3 of the British type isolate (Blencowe strain) of tomato aspermy virus. Virus Genes 8, 79–81.

Otwinowski, Z., Minor, W., 1997. Processing of X-ray diffraction data collected in oscillation mode. In: Carter, J.W.M.J., Sweet, R.M. (Eds.), Methods Enzymology Macromolecular Crystallography. Academic Press, San Diego, pp. 307–326.

Savithri, H.S., Devarajan, S., Murthy, M.R.N., 1984. Stability and structural transitions of tomato aspermy virus and cucumber mosaic virus. Virology 134, 398–405.

Smith, T.J., Chase, E., Schmidt, T., Perry, K.L., 2000. The structure of cucumber mosaic virus and comparison to cowpea chlorotic mottle virus. J. Virol. 74, 7578–7586.

Speir, J.A., Munshi, S., Wang, G., Baker, T.S., Johnson, J.E., 1995. Structures of the native and swollen forms of cowpea chlorotic mottle virus determined by X-ray crystallography and cryo-electron microscopy. Structure 3, 63–78.

Stehle, T., Harrison, S.C., 1996. Crystal structures of murine polyomavirus in complex with straight-chain and branched-chain sialyloligosaccharide receptor fragments. Structure 4, 183–194.

Van Regenmortel, M.H.V., Fauquet, C.M., Bishop, D.H.L., Carstens, E.B., Estes, M.K., Lemon, S.M., Maniloff, J., Mayo, M.A., McGeoch, D.J., Pringle, C.R., Wickner, R.B., 2000. Virus Taxonomy: Seventh Report of the International Committee on Taxonomy of Viruses. Academic Press, San Diego.

Weiss, M.S., 2001. Global indicators of X-ray data quality. J. Appl. Crystallogr. 34, 130–135.

Wikoff, W.R., Tsai, C.J., Wang, G., Baker, T.S., Johnson, J.E., 1997. The structure of cucumber mosaic virus: cryoelectron microscopy, X-ray crystallography, and sequence analysis. Virology 232, 91–97.